Supporting Information

Dendritic porous yolk@ordered mesoporous shell structured heterogeneous nanocatalysts with enhanced stability

Xin Du,* *Caixia Zhao*, *Yi Luan*,* *Changbin Zhang*, *Mietek Jaroniec*, *Hongwei Huang*, *Xueji Zhang*, and *Shi-Zhang Qiao**

Dr. X. Du, C. Zhao, Prof. Y. Luan, Prof. X. Zhang

Research Center for Bioengineering and Sensing Technology,

School of Chemistry & Biological Engineering,

Beijing Key Laboratory for Bioengineering and Sensing Technology,

University of Science & Technology Beijing, Beijing 100083, P. R. China

E-mail: duxin@ustb.edu.cn, yiluan@ustb.edu.cn

Dr. X. Du, Prof. S. Z. Qiao

School of Chemical Engineering,

The University of Adelaide, Adelaide, SA 5005, Australia

E-mail: s.qiao@adelaide.edu.au

Prof. C. Zhang

Research Center for Eco-Environmental Sciences,

Chinese Academy of Sciences, Beijing 100085, China

Prof. M. Jaroniec

Department of Chemistry and Biochemistry,

Kent State University, Kent, Ohio 44242, USA

Dr. H. Huang

School of Materials Science and Technology,

China University of Geosciences, Beijing 100083, China

Table S1. Comparison of the turnover frequency (TOF) of various Au-loaded nanocatalysts for the reduction of 4-NP.

Catalysts	4-NP (μmol)	Time (min)	Au content (μmol))	TOF[a] (min^{-1})	Ref.
Au@meso-SiO_2 hollow nanospheres	0.0625	20	-	ca. 0.08	1
Au(21 nm)@HMSM yolk-shell catalyst	0.2	30	-	ca. 0.63	2
Au@[Na]-HMAS	30	12	-	ca. 1.1	3
Au@hollow-SiO_2@PSS catalyst	0.06	16	$3*10^{-3}$	1.0	4
Yolk-shell SiO_2@Au/PEGDMA	0.1	50	0.92×10^{-3}	2.2	5
Au@hollow SiO_2	0.24	25	0.2	0.05	6
Au NPs/silica nanotubes	3.6	14/3	0.934	0.826	7
Hollow tubular SiO_2-Au	0.3	6	6.09×10^{-2}	0.82	8
Fe_3O_4@SiO_2-Au@mSiO_2	0.5	15	3.4×10^{-1}	0.1	9
Double-shell TiO_2/SiO_2-Au	0.3	9	2.66×10^{-2}	1.25	10
Au(5 nm)-γ-Fe_2O_3	8	2	1.52	2.6	11
Fe_3O_4@Au-TiO_2/ZrO_2	34	6	1.59	3.56	12
hollow porous gold nanoparticles	0.3	9	2.14×10^{-2}	1.56	13
Yolk-shell Au@Fe_3O_4	0.4	5/3	<0.1015	>2.36	14
Au-GO hybrid	0.2	6	3×10^{-2}	1.11	15
Au@C yolk-shell	0.025	10	-	ca. 0.0025	16
PDA-Au/graphene	1.0	13	0.2	0.38	17
Au@hollow graphene nanoshell	100	3	30	1.12	18
Au NPs/ polyacrylonitrile	86.5	210	-	1.42	19
Fe_3O_4@PDA-Au	0.85	19	1.09×10^{-2}	4.1	20
Poly(DVB-co-AA) @Au	39.1	72	0.147	3.7	21
DPSSs@Au NPs@MSS (35 nm)	**2.5**	**8**	**8.63×10^{-2}**	**3.62**	**This work**

[a] Calculated by the moles of the reduced 4-NP/the mole of Au content/the consumed time.

Supplementary Results

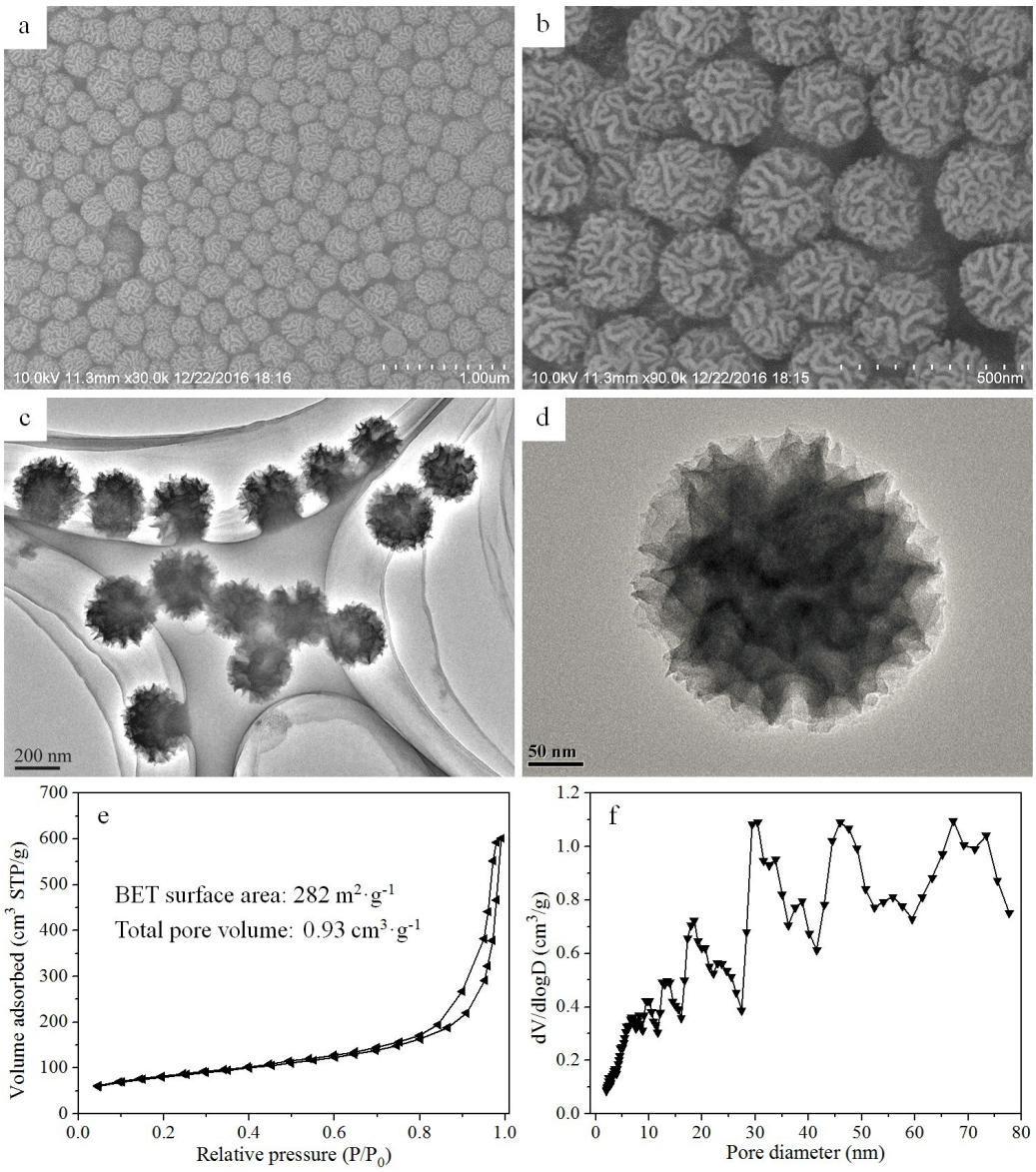

Fig. S1. SEM (a,b) and TEM (c,d) images of DPSSs. (e) N_2 sorption isotherm measured on the synthesized DPSSs and (f) the corresponding pore size distribution curve determined by using the Quenched Solid Density Functional Theory (QSDFT) method using nitrogen adsorption data.

DPSSs have the high BET surface area of 282 $m^2 \cdot g^{-1}$ and total pore volume of 0.93 $cm^3 \cdot g^{-1}$. The corresponding pore size distribution curve shows several peaks (Fig. S1f), which further validates the wide pore size distribution of DPSSs.

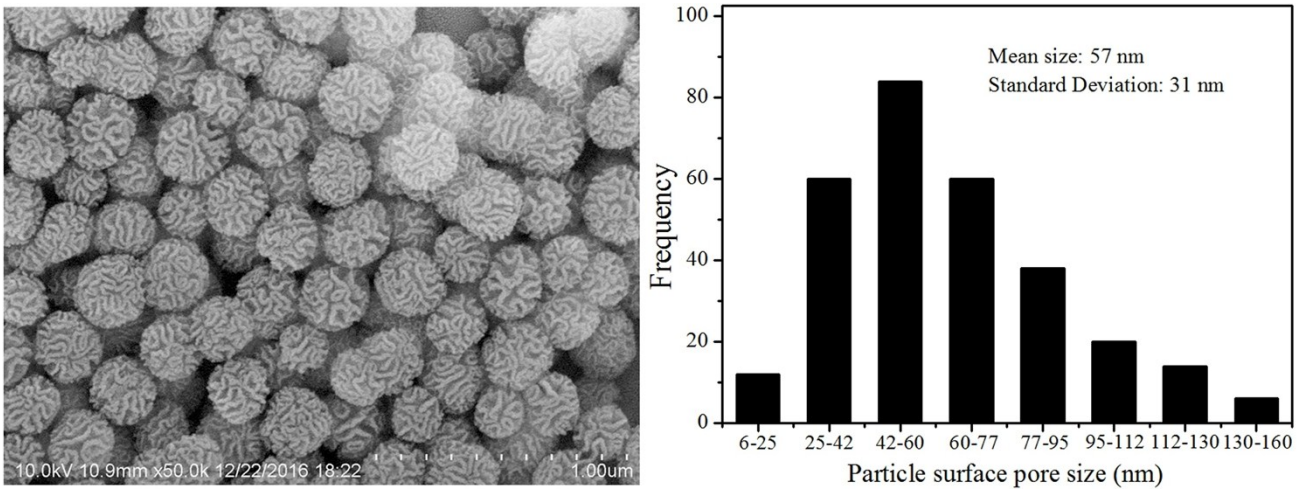

Fig. S2. SEM image of DPSSs and distribution histogram of pore sizes of DPSSs particle surface.

It should be noted that the center-radial large pores, which are composed of wrinkled nanosheets, are irregular slit-like pores with wide surface pore size distribution of 57±31 nm.

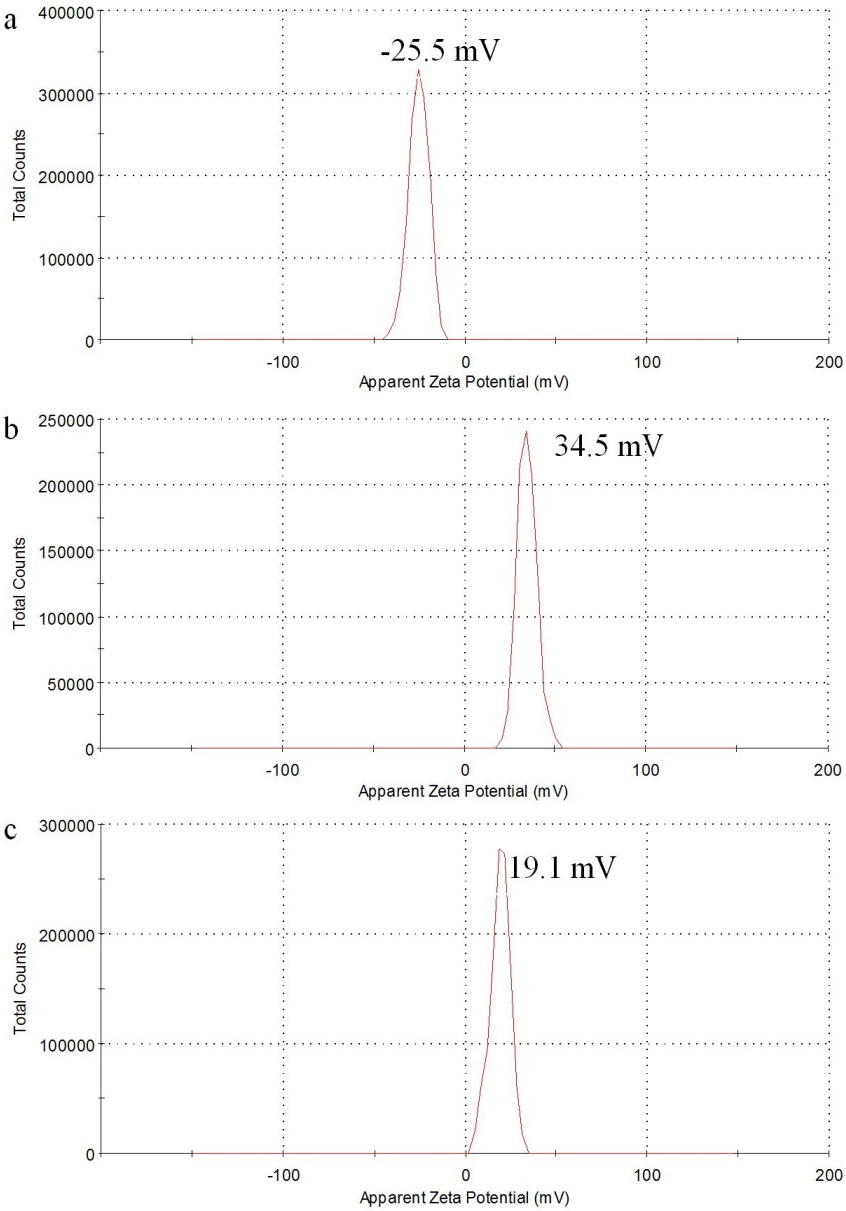

Fig. S3. Zeta potentials of DPSSs (−25.5 mV), DPSSs-NH_2 (+34.5 mV), and DPSSs-NH_2@Au NPs (+19.1 mV) dispersed in water at room temperature, which were measured by using dynamic light scattering.

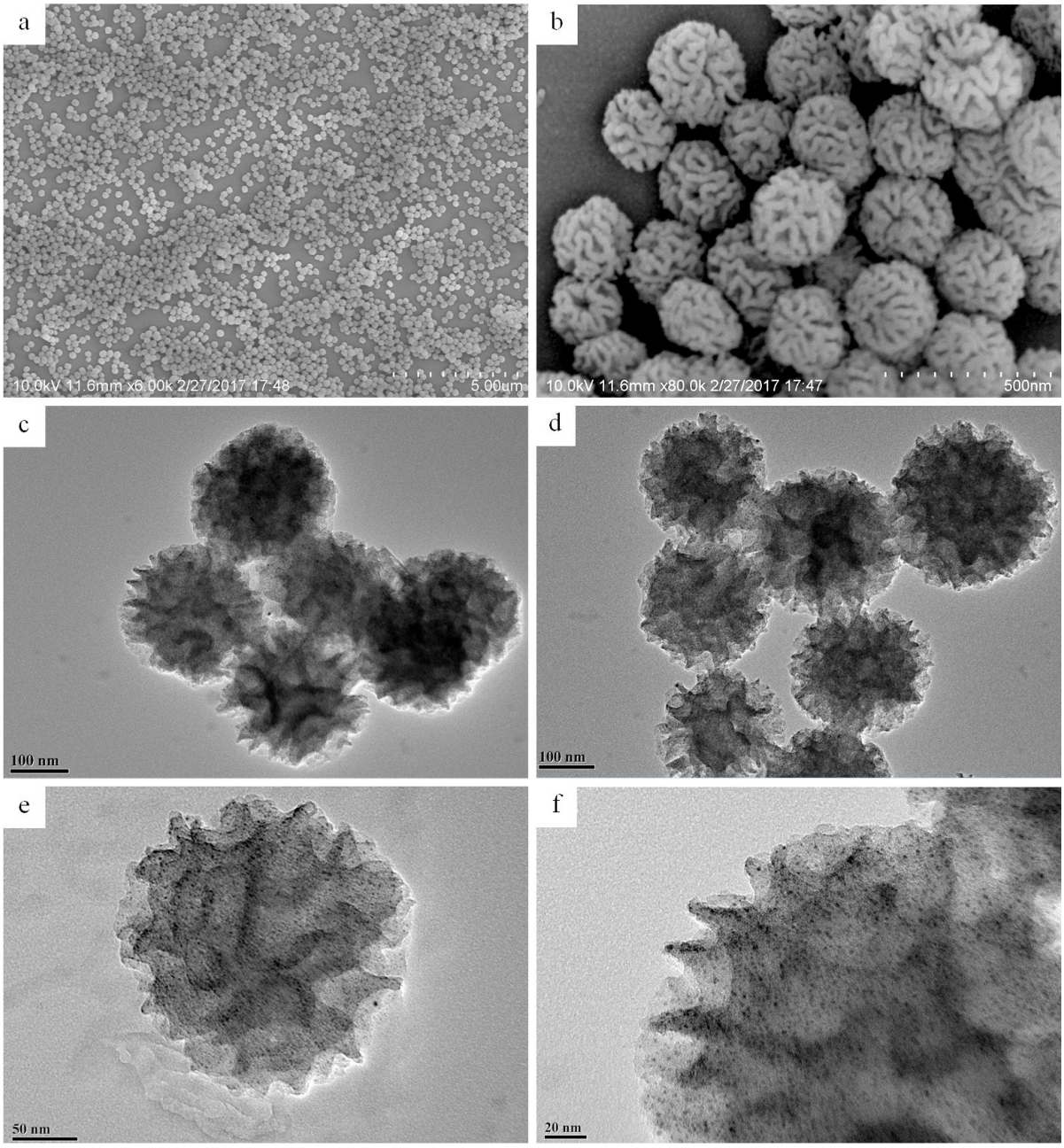

Fig. S4. SEM (a,b) and TEM (c-f) images of DPSSs-NH_2@Au NPs.

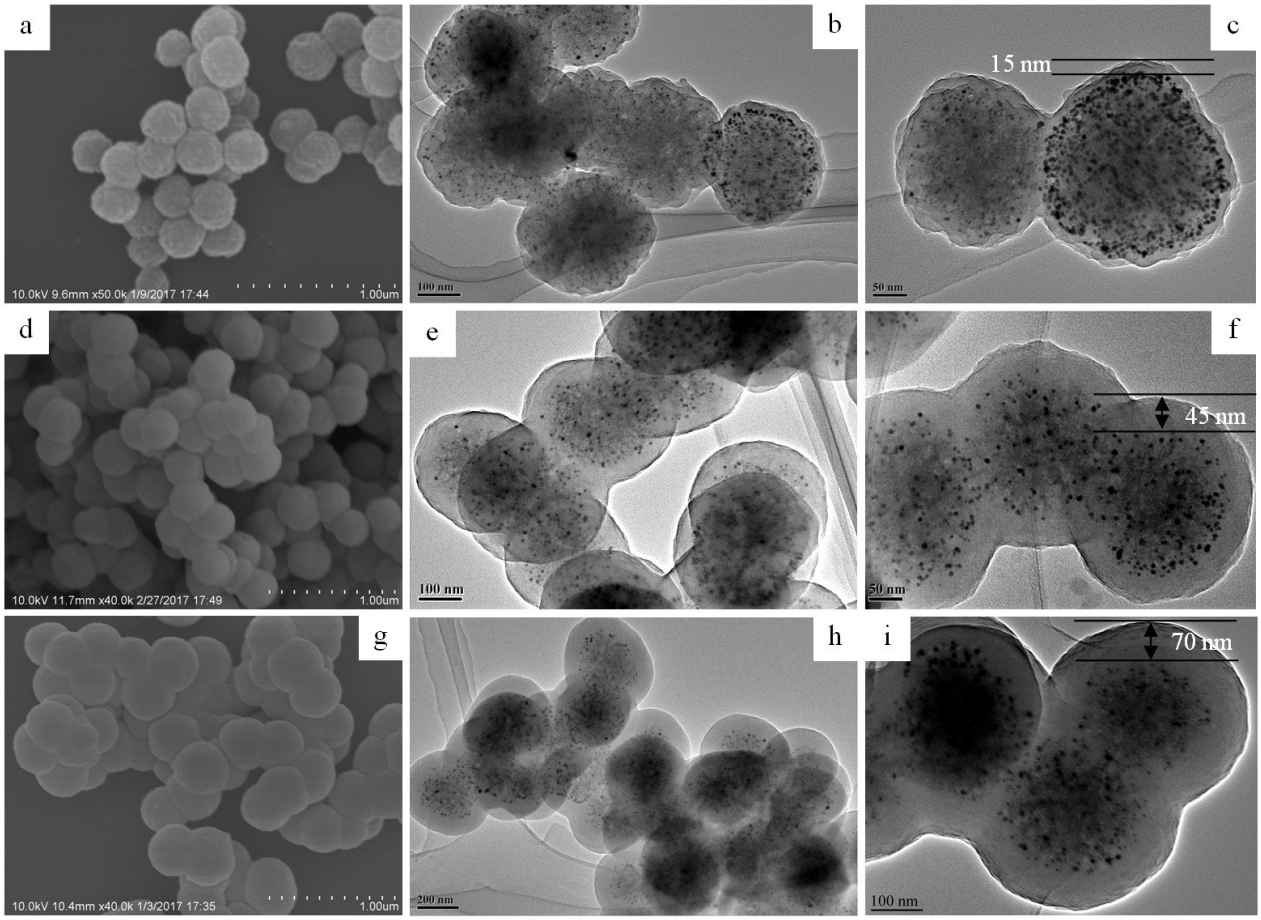

Fig. S5. SEM (a,d,g) and TEM (b,c,e,f,h,i) images of DPSSs-NH_2@Au NPs@RF with tunable RF layer thickness.

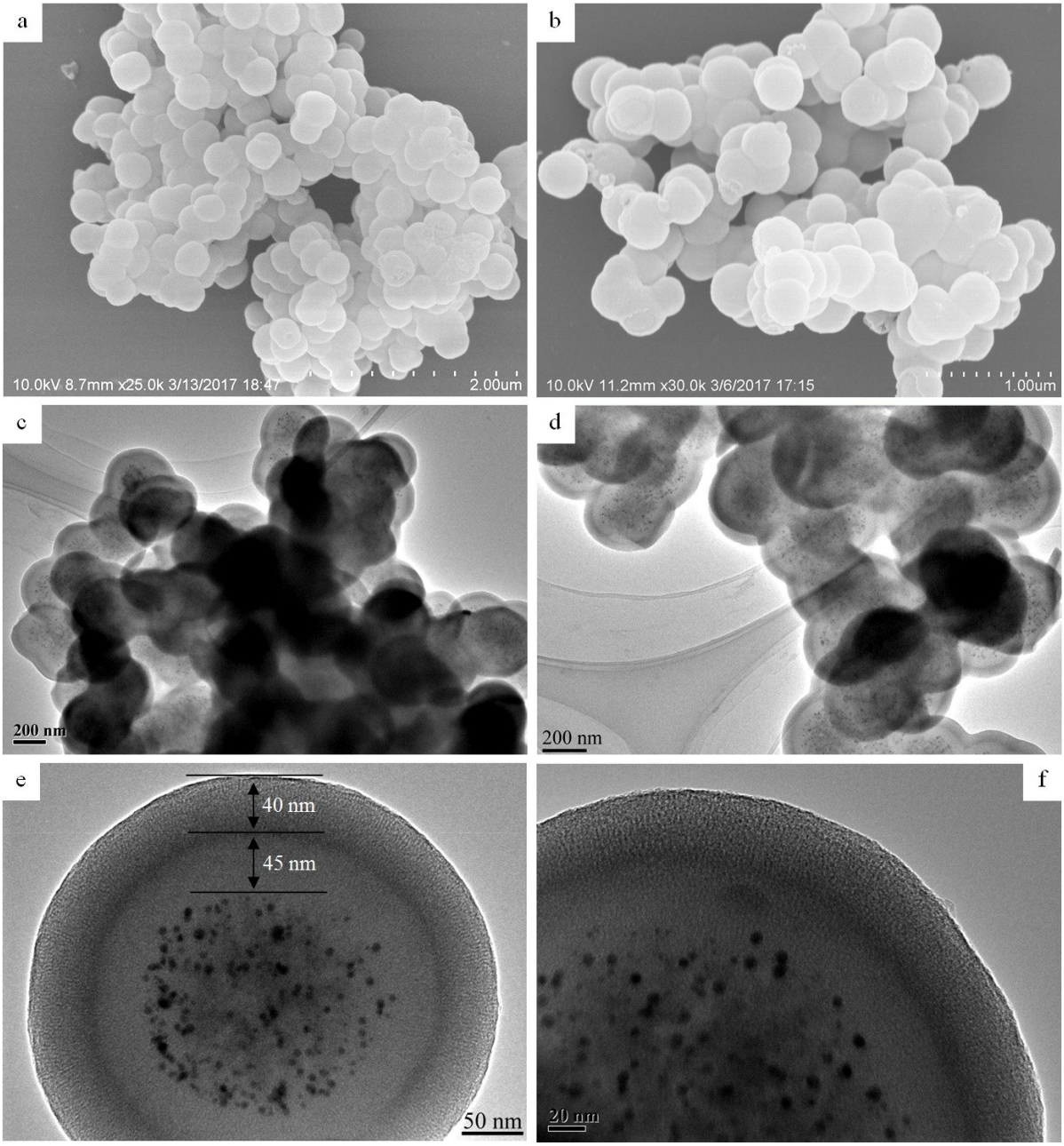

Fig. S6. SEM (a,b) and TEM (c-f) images of DPSSs-NH_2@Au NPs@RF@MSS.

MSS has a uniform thickness size.

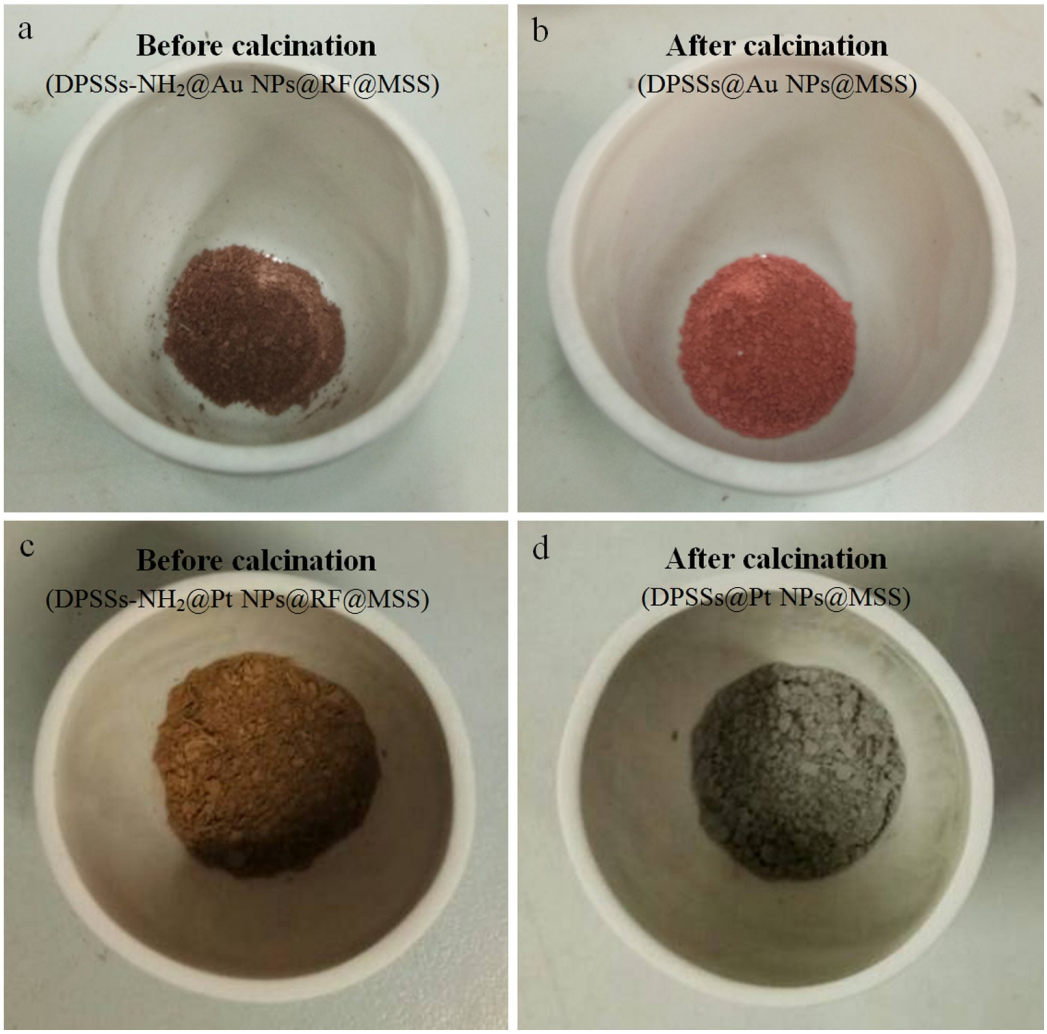

Fig. S7. Digital pictures of DPSSs-NH_2@Au NPs@RF@MSS (a), DPSSs@Au NPs@MSS (b), DPSSs-NH_2@Pt NPs@RF@MSS (c) and DPSSs@Pt NPs@MSS (d).

After calcination, the light red color of DPSSs@Au NPs@MSS product suggests small size of Au NPs, and the gray color DPSSs@Pt NPs@MSS product indicates the formation of nanosized Pt NPs.[1]

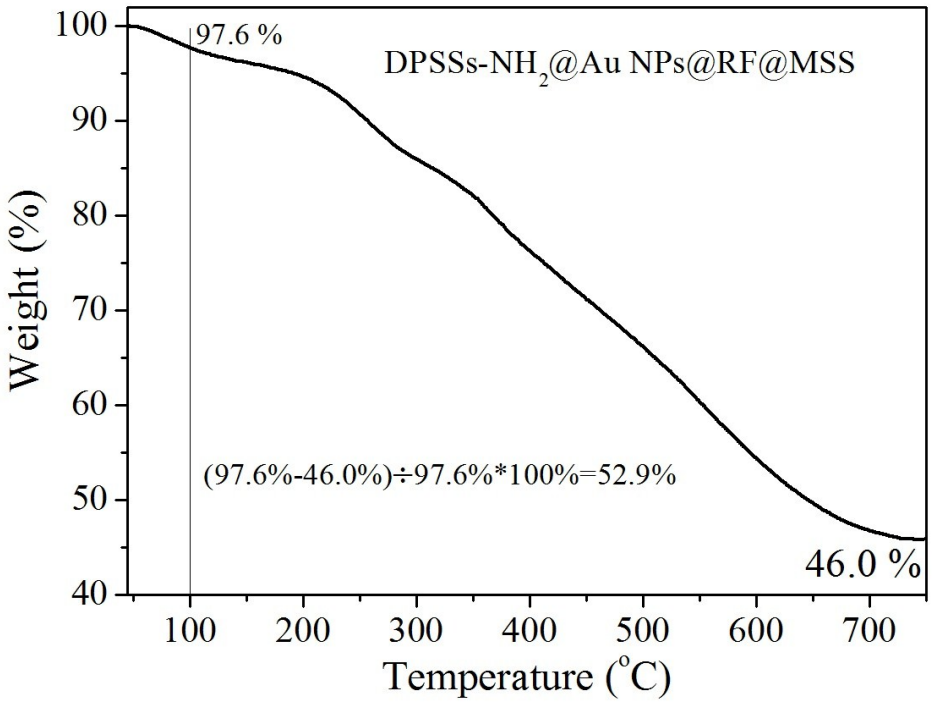

Fig. S8. TGA curve of DPSSs-NH_2@Au NPs@RF (shell thickness: ca. 45 nm)@MSS at a heating rate of 10 $^{o}C \cdot min^{-1}$ under a flow of air gas.

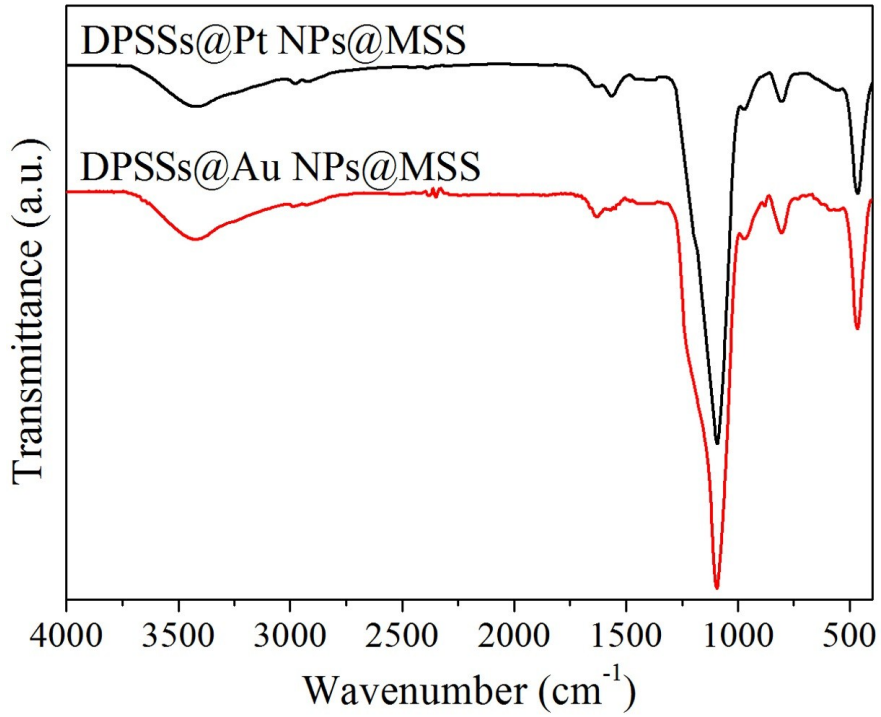

Fig. S9. FTIR spectra of DPSSs@Au NPs@MSS and DPSSs@Pt NPs@MSS obtained after calcinations at 550 ^{o}C for 6 h.

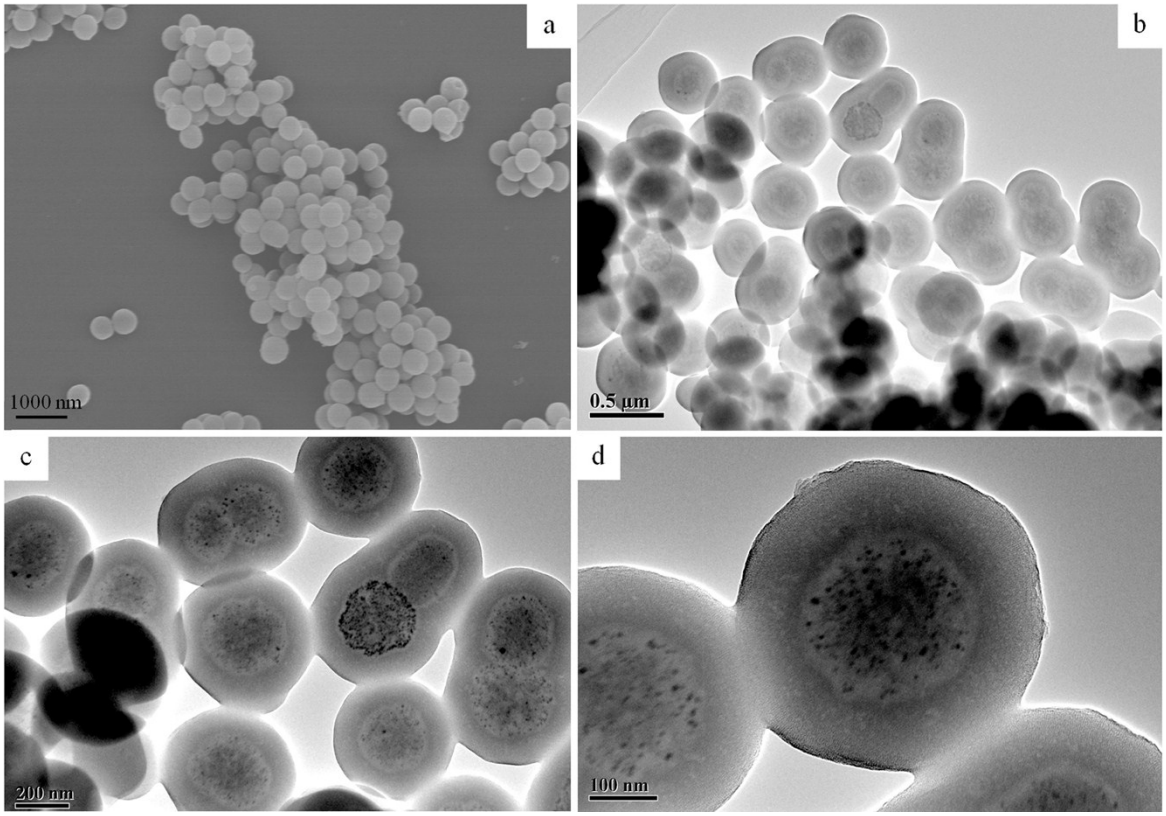

Fig. S10. TEM images of DPSSs@Au NPs@MSS with a shell thickness of ca. 95 nm.

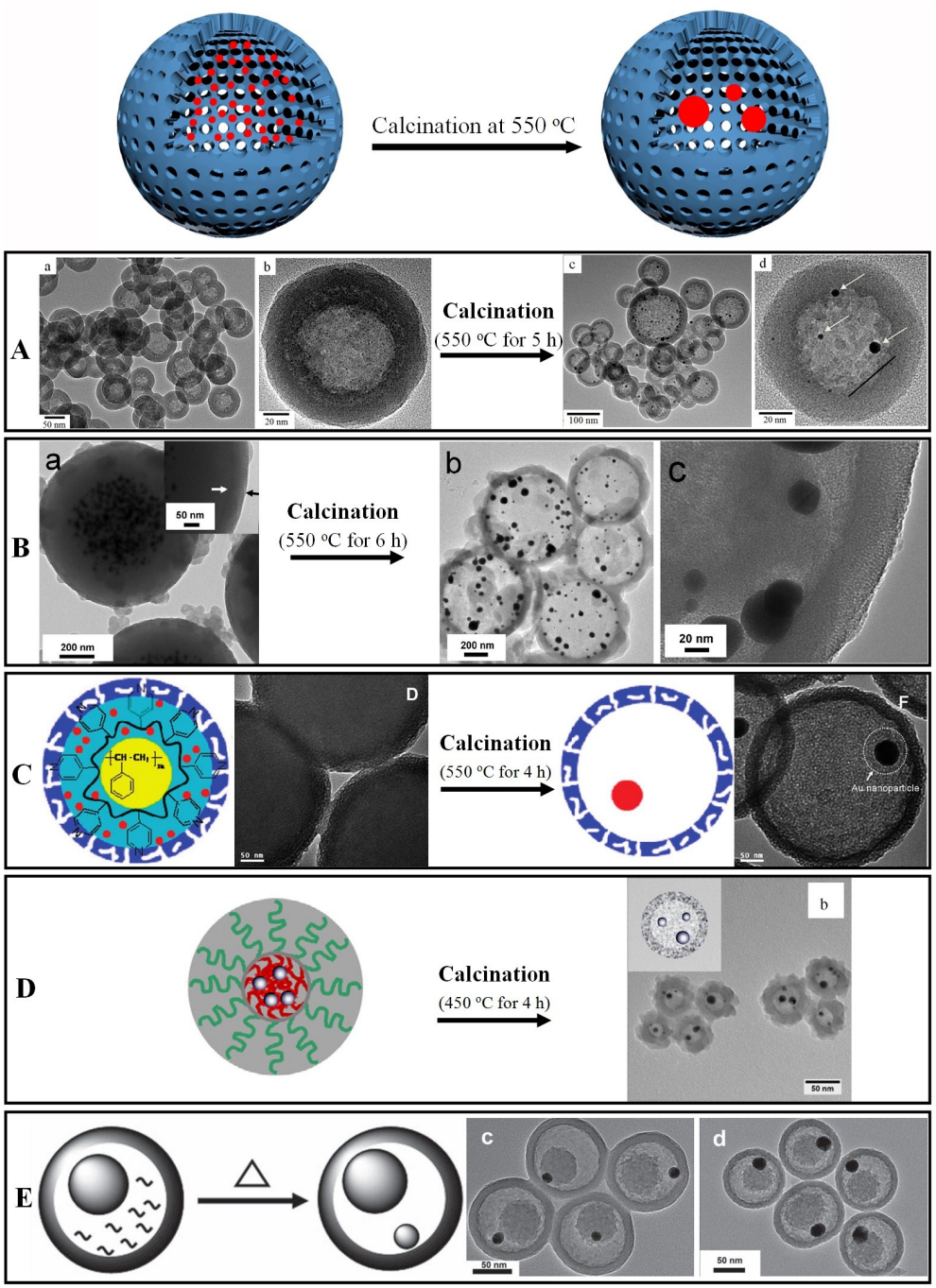

Fig. S11. Schematic illustration of thermally-induced aggregation of Au NPs encapsulated in hollow cavity. TEM images of samples before and after thermal treatment: (A) yolk-shell Au NPs@hollow silica nanospheres (HSNs),[22] (B) core–shell Au@RF@meso-SiO_2 nanospheres,[1] (C) Au NPs@PS-*co*-P4VP@hollow mesoporous silica nanospheres (HMSNs),[2] (D) Au NPs@PS-*co*-P4VP@HSNs[4] and (E) yolk-shel silica nanospheres containing $HAuCl_4$.[23] Reprinted with permission from Ref. [1,2,4,22,23]. Copyright 2014 Elsevier,[1] Copyright 2011 American Chemical Society,[2] Copyright 2017 Elsevier,[4] Copyright 2012[22] and 2011[23] Wiley-VCH.

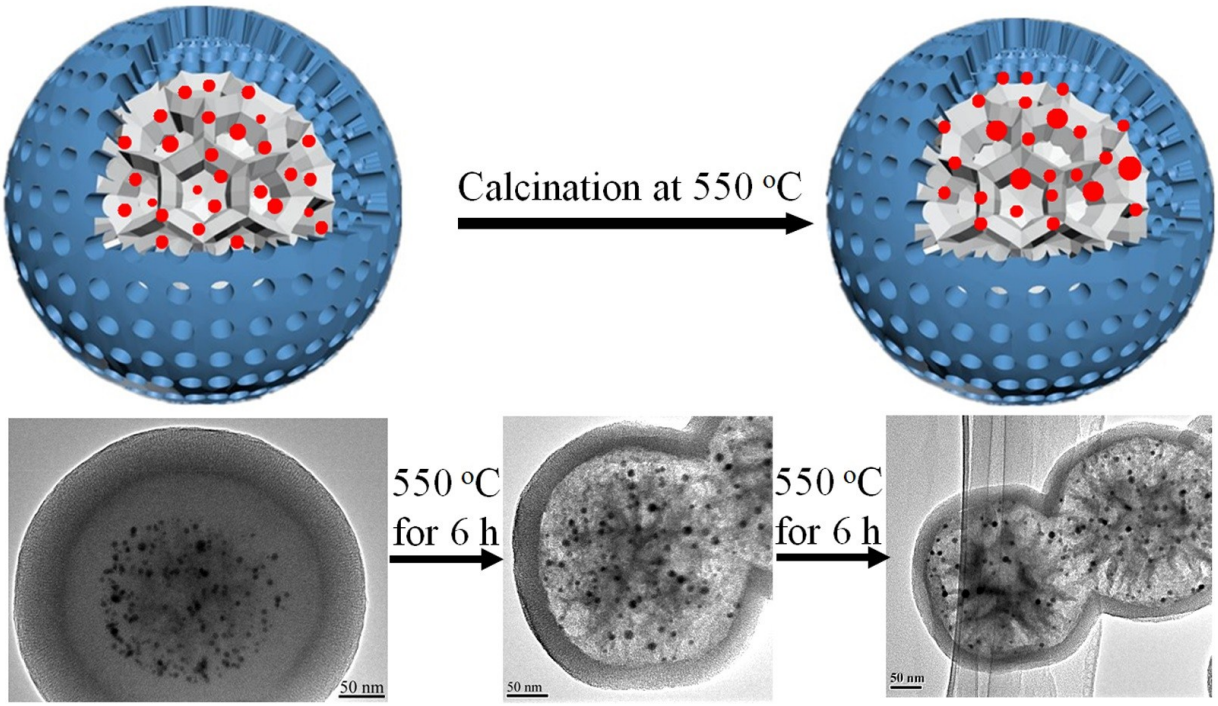

Fig. S12. Schematic illustration and TEM images of integrated nanostructures of dendritic porous yolk@noble metal NPs@MSS efficiently suppressing Ostwald ripening aggregation of noble metal NPs under high temperature.

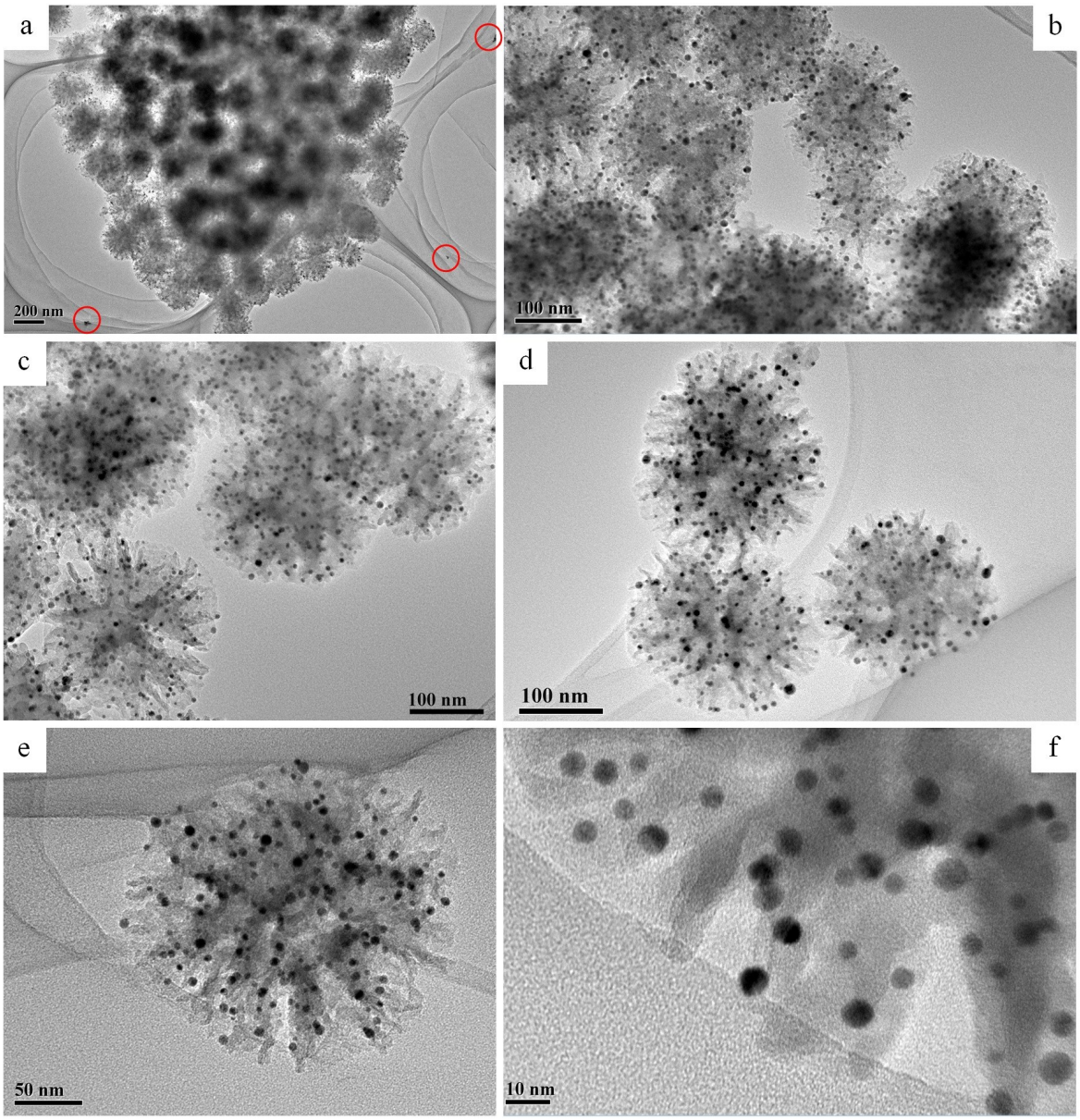

Fig. S13. TEM images of DPSSs@Au NPs after calcination of DPSSs-NH_2@Au NPs at 550 ^oC for 6 h.

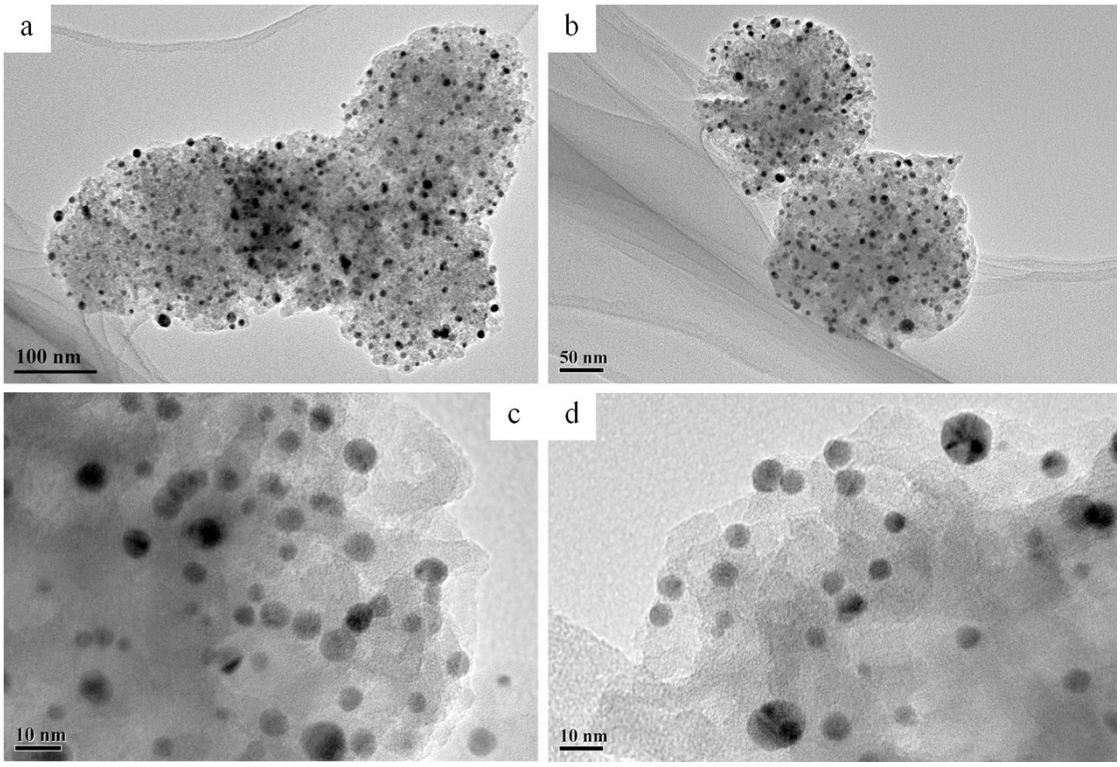

Fig. S14. TEM images of DPSSs@Au NPs after calcination of DPSSs-NH_2@Au NPs at 650 ^oC for 6 h.

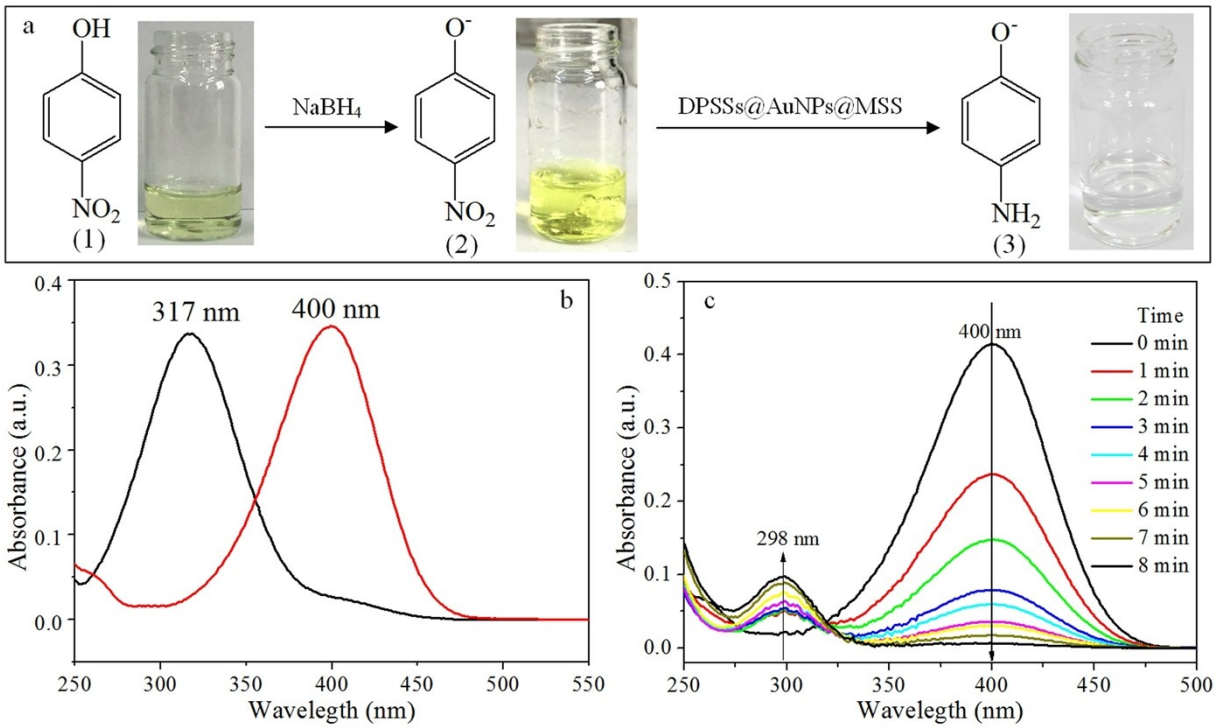

Fig. S15. (a) Deprotonation of 4-NP after addition of $NaBH_4$ solution and its subsequent catalytic reduction after addtion of DPSSs@Au NPs@MSS with a shell thickness of ca. 35 nm. (b) UV-vis spectra of 4-NP before and after addition of $NaBH_4$. (c) Time-dependent absorption spectra of the reaction solution.

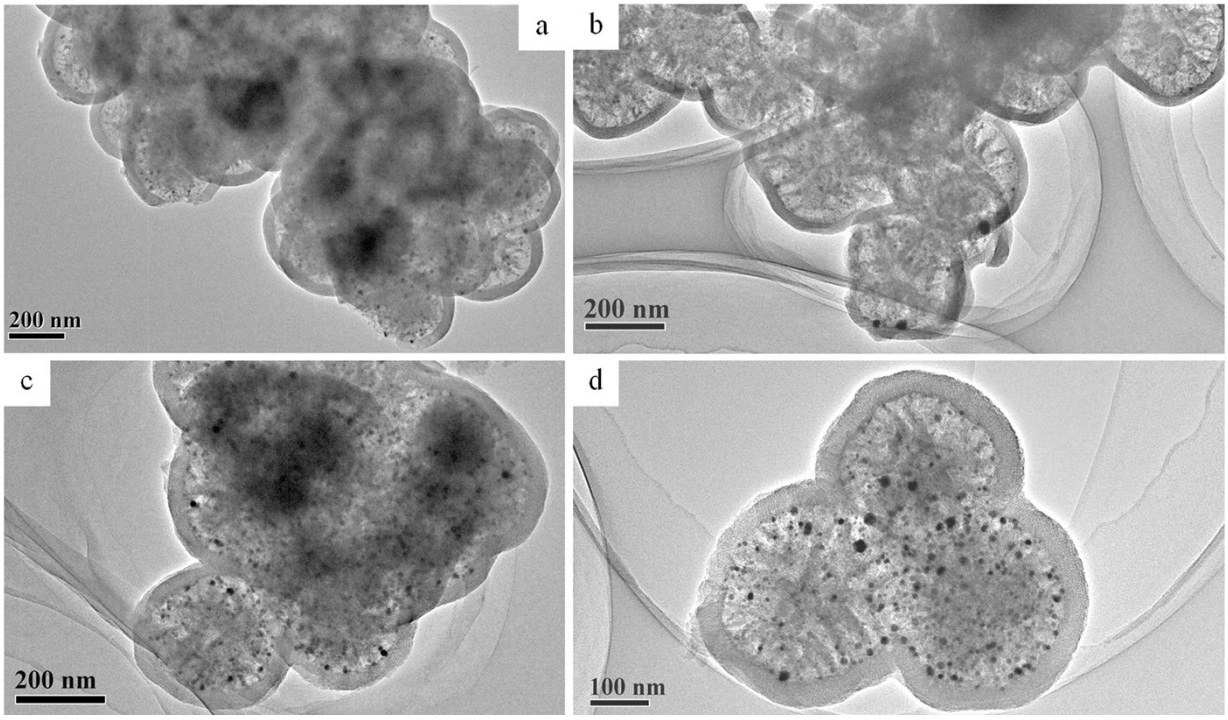

Fig. S16. TEM images of DPSSs@Au NPs@MSS after 10 repeated catalytic tests.

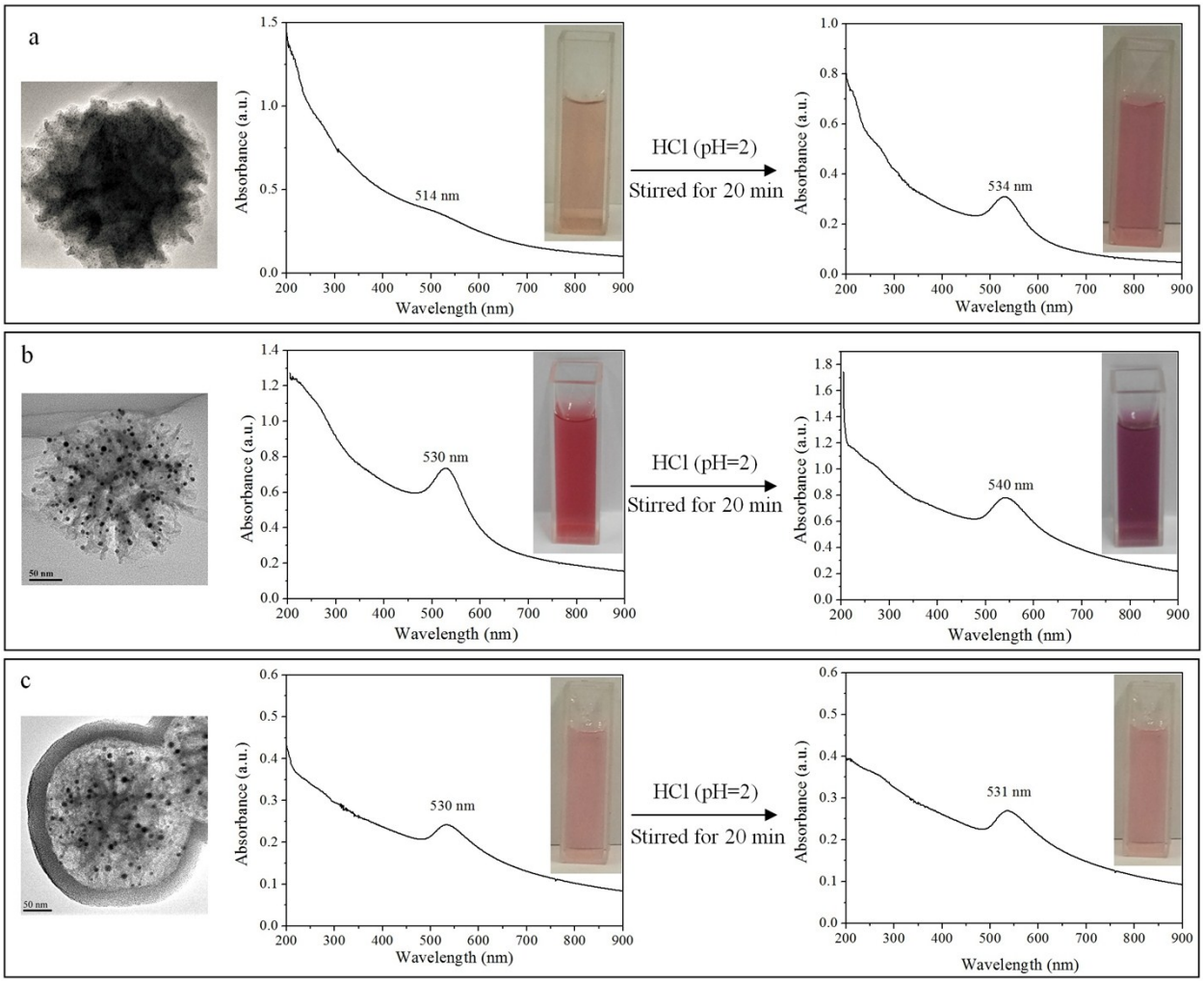

Fig. S17. UV-vis absorption spectra of DPSSs-NH_2@Au NPs (a), DPSSs @Au NPs (after calcination at 550 ^oC for 6 h) and DPSSs@Au NPs@MSS with a shell thickness of ca. 35 nm (b) suspensions before and after treatment with HCl solution (pH = 2) for 20 min.

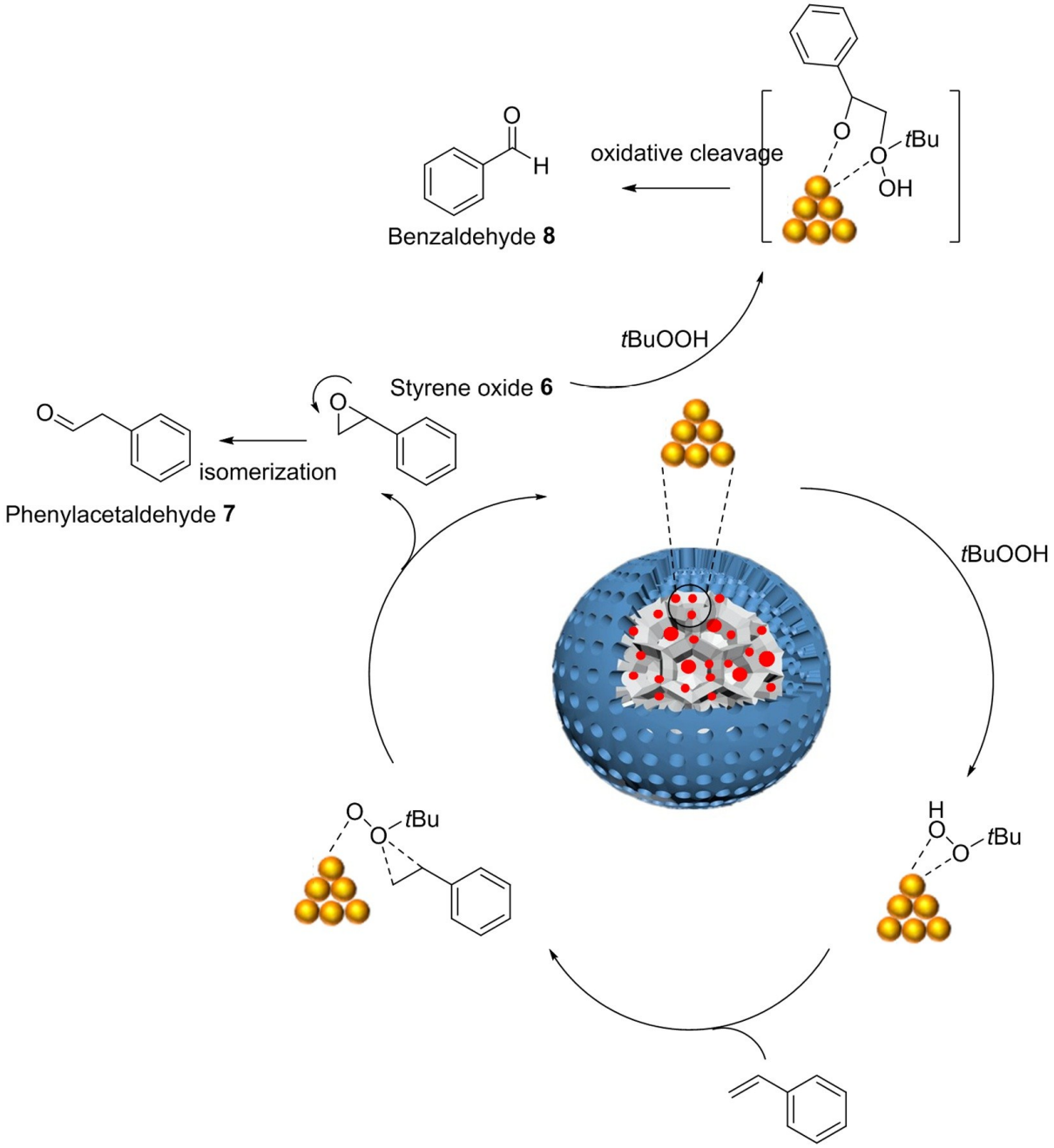

Fig. S18. Proposed mechanism for the styrene epoxidation. The kinetic styrene oxide product can be further converted to be thermodynamic benzaldehyde product.

Reference:

[1] J. Chen, Z. Xue, S. Feng, B. Tu, D. Zhao, Synthesis of mesoporous silica hollow nanospheres with multiple gold cores and catalytic activity, *J. Colloid Interface Sci.* **2014**, *429*, 62–67.

[2] S. Wang, M. Zhang, W. Zhang, Yolk-Shell Catalyst of Single Au Nanoparticle Encapsulated within Hollow Mesoporous Silica Microspheres, *ACS Catal.* **2011**, *1*, 207–211.

[3] X. Fang, Z. Liu, M. F. Hsieh, M. Chen, P. Liu, C. Chen, N. Zheng, Hollow Mesoporous Aluminosilica Spheres with Perpendicular Pore Channels as Catalytic Nanoreactors, *ACS Nano* **2012**, *6*, 4434–4444.

[4] A. Shajkumar, B. Nandan, S. Sanwaria, V. Albrecht, M. Libera, M. H. Lee, G. Auffermann, M. Stamm, A. Horechyy, Silica-supported Au@hollow-SiO_2 particles with outstanding catalytic activity prepared via block copolymer template approach, *J. Colloid Interface Sci.* **2017**, *491*, 246–254.

[5] B. Liu, W. Zhang, H. Feng, X. Yang, Rattle-type microspheres as a support of tiny gold nanoparticles for highly efficient catalysis, *Chem. Commun.* **2011**, *47*, 11727–11729.

[6] S. H. Wu, C. T. Tseng, Y. S. Lin, C. H. Lin, Y. Hung, C. Y. Mou, Catalytic nano-rattle of Au@hollow silica: towards a poison-resistant nanocatalyst, *J. Mater. Chem.* **2011**, *21*, 789–794.

[7] Z. Zhang, C. Shao, P. Zou, P. Zhang, M. Zhang, J. Mu, Z. Guo, X. Li, C. Wang, Y. Liu, In situ assembly of well-dispersed gold nanoparticles on electrospun silica nanotubes for catalytic reduction of 4-nitrophenol, *Chem. Commun.* **2011**, *47*, 3906–3908.

[8] S. Xiang, Y. Zhou, Y. Zhang, Z. Zhang, X. Sheng, S. Zhou, Z. Yang, A highly reactive and enhanced thermal stability nanocomposite catalyst based on Au nanoparticles assembled in the inner surface of SiO_2 hollow nanotubes, *Dalton Trans.* **2014**, *43*, 11039–11047.

[9] Y. Deng, Y. Cai, Z. Sun, J. Liu, C. Liu, J. Wei, W. Li, C. Liu, Y. Wang, D. Zhao, Multifunctional mesoporous composite microspheres with well-designed nanostructure: a highly integrated catalyst system, *J. Am. Chem. Soc.* **2010**, *132*, 8466–8473.

[10] J. Fang, Y. Zhang, Y. Zhou, C. Zhang, S. Zhao, H. Zhang, X. Sheng, In-situ construction of Au nanoparticles confined in double-shelled TiO2/mSiO2 hollow architecture for excellent catalytic activity and enhanced thermal stability, *Appl. Surf. Sci.* **2017**, *392*, 36–45.

[11] L. Shang, Y. Liang, M. Li, G. I. N. Waterhouse, P. Tang, D. Ma, L. -Z. Wu, C.-H. Tung, T. Zhang, "Naked" Magnetically Recyclable Mesoporous Au–γ-Fe_2O_3 Nanocrystal Clusters: A Highly Integrated Catalyst System, *Adv. Funct. Mater.* **2017**, *27*, 1606215.

[12] H. Zhang, Y. Zhang, Y. Zhou, C. Zhang, M. Zhang, S. Zhao, J. Fang, X. Sheng, Preparation of magnetically recoverable gold nanocatalysts with a highly reactive and enhanced thermal stability. *J. Alloy. Compd.* **2016**, *688*, 23–31.

[13] M. Guo, J. He, Y. Li, S. Ma, X. Sun, One-step synthesis of hollow porous gold nanoparticles with tunable particle size for the reduction of 4-nitrophenol, *J. Hazard. Mater.* **2016**, *310*, 89–97.

[14] F. Lin, R. Doong, Catalytic Nanoreactors of Au@Fe_3O_4 Yolk−Shell Nanostructures with Various Au Sizes for Efficient Nitroarene Reduction, *J. Phys. Chem. C* **2017**, *121*, 7844−7853.

[15] Y. Song, J. Lu, B. Liu, C. A Lu, facile construction of Au nanoparticles on a copolymer ligand brushes modified graphene oxide nanoplatform with excellent catalytic properties, *RSC Adv.* **2016**, *6*, 64937–64945.

[16] R. Liu, F. Qu, Y. Guo, Nan Yao, R. D. Priestley, Au@carbon yolk–shell nanostructures via one-step core–shell–shell template, *Chem. Commun.* **2014**, *50*, 478–480.

[17] J. Luo, N. Zhang, R. Liu, X. Liu, In situ green synthesis of Au nanoparticles onto polydopamine-functionalized graphene for catalytic reduction of nitrophenol, *RSC Adv.* **2014**, *4*, 64816–64824.

[18] H. Liu, J. Wang, Z. Feng, Y. Lin, L. Zhang, D. Su, Facile synthesis of Au nanoparticles embedded in an ultrathin hollow graphene nanoshell with robust catalytic performance, *Small* **2015**, 11, 5059–5064.

[19] Y. Liu, G. Jiang, L. Li, H. Chen, Q. Huang, T. Jiang, X. Du, W. Chen, Preparation of Au/PAN nanofibrous membranes for catalytic reduction of 4-nitrophenol, *J. Mater. Sci.* **2015** , 50, 8120–8127.

[20] T. Zeng, X. L. Zhang, H. Y. Niu, Y. R. Ma, W. H. Li, Y. Q. Cai, In situ growth of gold nanoparticles onto polydopamine-encapsulated magnetic microspheres for catalytic reduction of nitrobenzene, *Appl. Catal. B* **2013**, *134–135*, 26–33.

[21] W. Liu, X. Yang, W. Huang, Catalytic properties of carboxylic acid functionalized-polymer microsphere-stabilized gold metallic colloids, *J. Colloid Interface Sci.* **2006**, *304*, 160–165.

[22] X. Du, L. Yao, J. He, One-pot fabrication of noble-metal nanoparticles that are encapsulated in hollow silica nanospheres: dual roles of poly (acrylic acid), *Chem. Eur. J.* **2012**, *18*, 7878-7885.

[23] L. Tan, D. Chen, H. Liu, F. Tang, A Silica Nanorattle with a Mesoporous Shell: An Ideal Nanoreactor for the Preparation of Tunable Gold Cores, *Adv. Mater.* **2010**, *22*, 4885–4889.